The American Journal of Pathology, Vol. 181, No. 6, December 2012

http://dx.doi.org/10.1016/j.ajpath.2012.08.031

Biophysical Imaging and Computational Biology

Spectral Discrimination of Cerebral Amyloid Lesions after Peripheral Application of Luminescent Conjugated Oligothiophenes

Bettina M. Wegenast-Braun,*† Angelos Skodras,*† Gonca Bayraktar,*†‡ Jasmin Mahler,*†‡ Sarah K. Fritschi,*†‡ Therése Klingstedt,§ Jeffrey J. Mason,§ Per Hammarström,§ K. Peter R. Nilsson,§ Christian Liebig,*† and Mathias Jucker*†

From the Department of Cellular Neurology, Hertie Institute for Clinical Brain Research, and the Graduate School for Cellular and Molecular Neuroscience,‡ University of Tübingen, Tübingen, Germany; DZNE,† German Center for Neurodegenerative Diseases, Tübingen, Germany; and the Department of Chemistry,§ IFM, Linköping University, Linköping, Sweden*

***In vivo* imaging of pathological protein aggregates provides essential knowledge of the kinetics and implications of these lesions in the progression of proteopathies, such as Alzheimer disease. Luminescent conjugated oligothiophenes are amyloid-specific ligands that bind and spectrally distinguish different types of amyloid aggregates. Herein, we report that heptamer formyl thiophene acetic acid (hFTAA) passes the blood-brain barrier after systemic administration and specifically binds to extracellular β-amyloid deposits in the brain parenchyma (Aβ plaques) and in the vasculature (cerebral β-amyloid angiopathy) of β-amyloid precursor protein transgenic APP23 mice. Moreover, peripheral application of hFTAA also stained intracellular lesions of hyperphosphorylated Tau protein in P301S Tau transgenic mice. Spectral profiling of all three amyloid types was acquired *ex vivo* using two-photon excitation. hFTAA revealed a distinct shift in its emission spectra when bound to Aβ plaques versus Tau lesions. Furthermore, a spectral shift was observed for Aβ plaques versus cerebral β-amyloid angiopathy, indicating that different amyloid types and structural variances of a specific amyloid type can be distinguished. In conclusion, by adding spectral signatures to amyloid lesions, our results pave the way for a new area of *in vivo* amyloid imaging, allowing *in vivo* differentiation of amyloid (sub)types and monitoring changes of their structure/composition over time.** *(Am J Pathol 2012, 181: 1953–1960; http://dx.doi.org/10.1016/j.ajpath.2012.08.031)*

Amyloidosis is a common pathological hallmark of most age-related neurodegenerative diseases.[1,2] Each disease is characterized by the deposition of one or several proteins in the amyloid state in which they form elongated, unbranched fibers, with a core consisting of many stranded β-sheets. All amyloids share a common three-dimensional structure with similar chemical and biophysical properties.[3] Thereby, amyloids are specifically recognized by hydrophobic dyes, such as Congo red and thioflavin T,[4,5] that historically have been used for the histopathological diagnosis of amyloid diseases. On binding to amyloid, Congo red reveals a typical apple green birefringence (anomalous colors) under polarized light, whereas the fluorescence intensity of thioflavin T strongly increases on amyloid binding.[6]

More recently, Congo red and thioflavin T derivatives have been developed for *in vivo* amyloid imaging. For example, in Alzheimer disease (AD), Pittsburgh Compound B is used for the detection of Aβ deposits with positron emission tomography.[7] Pittsburgh Compound B–positron emission tomography imaging is thought to predict AD disease progression from a presymptomatic phase to symptomatic AD.[8,9] Methoxy-X04 has been used for multiphoton *in vivo* imaging of Aβ lesions in experimental mouse models,[10,11] and such imaging studies have greatly contributed to a better understanding of the dynamics of Aβ plaque formation and growth.[12]

Supported by European Union FP7 HEALTH [Project LUPAS (Luminescent Polymers for *in Vivo* Imaging of Amyloid Signatures)], an ERCStarting Independent Researcher Grant [Project MUMID (Multimodal Tools for Molecular Imaging, Diagnostics and Therapeutics) to K.P.R.N.], and the Swedish Foundation for Strategic Research (GrantFFL-4 to K.P.R.N.).

Accepted for publication August 9, 2012.

Address reprint requests to Bettina M. Wegenast-Braun, Ph.D. or Mathias Jucker, Ph.D., Department of Cellular Neurology, Hertie Institute for Clinical Brain Research, Otfried-Mueller Strasse 27, D-72076 Tuebingen, Germany. E-mail: bettina.braun@uni-tuebingen.de or mathias.jucker@uni-tuebingen.de.

Pittsburgh Compound B and methoxy-X04 can both be applied peripherally [ie, they cross the blood-brain barrier (BBB) reasonably well].

Despite the tremendous progress of *in vivo* amyloid imaging, several hurdles remain. Given the mixed pathological characteristics of most cerebral amyloidoses and the increasing interest in particular conformational variants (amyloid strains) with potentially diverse different biological activities, there is great demand to dissociate the various amyloid lesions and amyloid (sub) types.[3,13–15] AD, for example, is characterized by amyloid lesions in forms of extracellular Aβ plaques and intracellular Tau aggregates, so-called neurofibrillary tangles.[16] In addition, patients with AD frequently exhibit Aβ deposition in the vasculature, a feature known as cerebral β-amyloid angiopathy (CβAA).[17] Dyes that could discriminate between those lesions would be of enormous scientific and diagnostic value.

A novel group of amyloid-specific ligands that can provide a unique spectral signature for distinct amyloid structures has recently been developed.[18] Luminescent conjugated polythiophenes (LCPs) and luminescent conjugated oligothiophenes (LCOs) possess a flexible backbone that can adapt its conformation on binding to the respective amyloid target. Because this structural twist results in a change in the spectral properties, subtle differences in amyloid conformation/structure can be visualized using one identical probe. Different conformational states of Aβ deposits could be visualized by applying LCPs to histological postmortem preparations.[19] Moreover, Aβ deposits could be separated from neurofibrillary tangles on human AD autopsy tissue.[20] LCPs have also differentiated multiple prion strains on histological stainings.[21]

The aim of the present study was to further exploit these amyloid ligands and to transfer their implications into an *in vivo* setting. We thereby identified an LCO, hFTAA,[20] that fulfilled all necessary requirements for *in vivo* spectral amyloid imaging.

Materials and Methods

Mice

Aged depositing APP23 mice,[22] overexpressing human APP with the Swedish double mutation (K670N/M671L), were used to evaluate the staining of Aβ plaques and CβAA. Aged hemizygous and homozygous P301S Tau transgenic (tg) mice,[23] expressing human Tau with the P301S single mutation, were used to study the staining capacities for Tau aggregates. Both lines express the transgene under the control of the neuron-specific murine Thy-1 promoter element and were on a C57BL/6J background. Crosses of the two lines (hemizygous for both transgenes) were used to obtain mice with mixed pathological characteristics. Non-transgenic animals were used as controls. All procedures with animals were performed in compliance with protocols approved by the local animal use committee and university regulations.

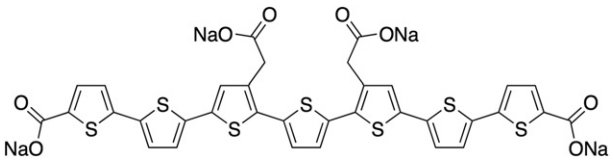

Figure 1. Chemical structure of the sodium salt of hFTAA.

In Vivo *Labeling and Tissue Processing*

Mice were i.v. injected once in the lateral tail vein with 20 mg/kg of the heptameric luminescent conjugated oligothiophene hFTAA,[20] dissolved at 5 mg/mL in PBS (the chemical structure of hFTAA is depicted in Figure 1). At 24 hours after injection, mice were sacrificed. For spectral analysis, one brain hemisphere was gently snap frozen by immersion in a 2-methylbutane bath surrounded by dry ice and stored at −80°C until it was coronally cut on a cryostat (Microm, Walldorf, Germany) in sections (25 μm thick) mounted on superfrost slides (R. Langenbrinck, Emmendingen, Germany). Slides were dried at room temperature and finally stored at −80°C. The day before spectral image acquisition, slides were thawed, dried at room temperature, and mounted with Fluorescence Mounting Medium (Dako, Carpentaria, CA). For overview images or immunohistochemical (IHC) staining, the other brain hemisphere was fixed in 4% paraformaldehyde in PBS for 2 days at 4°C, subsequently cryoprotected in 30% sucrose for another 2 days at 4°C, and frozen in 2-methylbutane. Coronal sections (40 μm thick) were taken using a freezing/sliding microtome (Leica, Nussloch, Germany). Sections were stored in cryoprotectant solution (25% glycerol and 30% ethylene glycol in 0.1 mol/L phosphate buffer) at −20°C. Before staining or mounting, sections were thoroughly washed in PBS.

Ex Vivo *Colocalization with Antibodies against Aβ and Tau Lesions*

Paraformaldehyde-fixed sections of hFTAA-injected mice were used for subsequent IHC labeling of Aβ and Tau aggregates using standard fluorescent immunolabeling procedures. For the non-fluorescence visualization of the Aβ signal, standard immunoperoxidase procedures were performed using an Elite ABC kit (Vector Laboratories, Burlingame, CA) and Vector SG (Vector Laboratories) as a substrate. In general, Aβ deposits were stained using the polyclonal antibody CN3 (1:1000) raised against synthetic human Aβ1–16 peptide.[24] Hyperphosphorylated Tau was detected with the monoclonal antibody AT100, specific to Tau phosphorylated at Ser212 and Thr214 (1:2000; Autogen Bioclear, Calne, UK). Alexa Fluor 633 goat anti-rabbit or goat anti-mouse IgGs (Invitrogen, Karlsruhe, Germany) were used as secondary antibodies, respectively. In contrast to CN3 labeling, Tau staining required an additional antigen retrieval step in 10 mmol/L citrate buffer (1.8 mmol/L citric acid and 8.2 mmol/L trisodium citrate, pH 6.0) at 90°C for 35 minutes. A semiquantitative analysis was performed to estimate the percentage of overlap between hFTAA and AT100 labeling.

Therefore, Tau labeling in the neocortex was analyzed on double-labeled sections (25 μm thick), two for each of the four P301S Tau tg mice (see *Results* for mice details). Two-channel images were acquired for randomly selected cortical AT100-positive cells. Image acquisition was performed at the Axioplan 2 fluorescent microscope coupled to a b/w MRm Axiocam (Carl Zeiss MicroImaging GmbH, Jena, Germany) using the YFP filter set (BP 500/20 for excitation and BP 535/30 for emission; AHF Analysentechnik, Tübingen, Germany) for hFTAA and the Cy5 filter set (BP 640/30 for excitation and BP 690/50 for emission; Carl Zeiss MicroImaging GmbH) for Alexa 633. After acquisition, all AT100-positive cells were visually examined for potential double labeling with hFTAA (in total, 198 cells were studied).

Histological Staining with Amyloidotropic Dyes

Staining with hFTAA (1.5 mmol/L in deionized water, diluted 1:500 in PBS) was performed similar to a previous description.[20] Staining with thioflavin S and Congo red was performed according to standard protocols. Staining with methoxy-X04 included incubation with a staining solution of 4% vol of 10 mg/mL methoxy-X04[10] in dimethyl sulfoxide and 7.7% vol CremophorEL (Sigma-Aldrich, Steinheim, Germany) in 88.3% vol PBS for 30 minutes at room temperature.

Image Acquisition

Mosaic overview images of hFTAA-injected mouse sections were acquired on a Zeiss Axioplan 2 fluorescent microscope with Axiocam MRm (Carl Zeiss MicroImaging GmbH) using the YFP filter set (BP 500/20 for excitation and BP 535/30 for emission; AHF Analysentechnik) and a 10×/0.3 air Plan Neofluar objective (Carl Zeiss MicroImaging GmbH) in combination with the MosaiX function of the Axiovision 4.7 software (Carl Zeiss MicroImaging GmbH). High-magnification images were acquired on either a Zeiss AxioImager.Z1 system [40×/1.3 oil Plan Apochromat objective; eGFP filter set (BP 470/40 for excitation and BP 525/50 for emission)] or a Zeiss LSM 510 META (Axiovert 200M) confocal microscope (20×/0.5 air Plan Neofluar objective, excitation at 488, emission collected using an LP505 filter). Images depicting hFTAA immunodouble labeling were taken with the Zeiss LSM 510 META (Axiovert 200M) confocal microscope. Laser lines 488 and 633 were used to excite hFTAA or Alexa Fluor 633, respectively. To depict the whole structure of interest, some images were acquired as stacks, and maximum-intensity projections are shown as indicated.

Two-Photon Imaging and Spectral Analysis

Mounted cryosections of hFTAA-injected depositing APP23 mice and hemizygous and homozygous P301S Tau tg mice were used for spectral analysis (for mice details, see *Results* and figure legends). To be consistent with *in vivo* settings/requirements, spectra were acquired using two-photon excitation. The used TCS SP2 MP microscope (Leica Microsystems, Mannheim, Germany) is equipped with a Spectra Physics Mai-Tai laser (tunable 710 to 990 nm), which was used for two-photon excitation at 780 nm (a pretest using different excitation wavelengths depicted superior excitability for hFTAA at this wavelength). A FemtoControl pulse compressor (APE, Berlin, Germany) was interposed in the beam path to potentiate the probability for a two-photon excitation event by shortening the pulse width, therefore enhancing signal intensity. For spectral imaging, the spectrophotometer detector was used, whereby the pinhole was completely opened. Emission scans were performed with 20-nm overlapping detection ranges, resulting in a final step size of 10 nm from 450 to 740 nm (30 steps in total) using the xyλ mode of the Leica confocal software (at a resolution of 256 × 256 pixels). To correct for possible bleaching effects, scans were also performed in the reverse direction (from 740 to 450 nm) and averaged afterward. Additional single-plane images were acquired at a higher resolution (512 × 512) to provide detailed morphological information. All imaging was performed using a ×40 HCX APO water-immersion objective (0.8 numerical aperture; Leica Microsystems).

Data Analysis and Statistics

Analysis of emission spectra was performed using the multimeasure analysis tool in ImageJ version 1.44e (*http://rsbweb.nih.gov/ij*, last accessed February 2012). Regions of interest (ROIs) were drawn around hFTAA-stained plaques, CβAA, and Tau-positive cells. Single images of the spectral emission scans were treated as stacks, and a maximum projection was used to place the respective ROIs. Care was taken to exclude areas of incomplete staining and, therefore, to minimize the contribution of autofluorescence. For Tau, additional care was taken to exclude areas with lipofuscin autofluorescence. Nevertheless, if a verifiable contribution of lipofuscin was observed in Tau spectral profiles, those were discarded, because this would have resulted in an artificial increase of the observed spectral shift. For each ROI, the corresponding mean gray values were measured. These data were further analyzed, whereby for each spectrum, the minimal signal was subtracted to exclude background signal, and the resulting values were normalized to the respective maximum. For each lesion type and scan direction, the mean was calculated, before averaging the values of the two scan directions to exclude bleaching effects. The resulting mean curves were again normalized. For further analysis, the spectral similarity of individual spectra was determined against the mean hFTAA plaque spectra using the spectral angle mapper (SAM) algorithm.[25–27] Spectral similarity values of hFTAA plaque spectra were then compared with hFTAA Tau or CβAA spectra using nonparametric statistics (*U*-test). Box plot whiskers denote the 10th and 90th percentiles. To visualize spectral differences within the two-photon images, all pixels of the acquired emission scan were assigned to a specific class (namely,

plaque, CAA, Tau, or background), according to the similarity of their spectral profiles to the respective reference spectra. A median filter of one pixel radius was applied where deemed necessary, to remove noisy pixels introduced by our system. Spectral similarity was again determined using the SAM algorithm. Normalization of the images was not necessary because SAM is independent of signal intensity. In detail, we implemented the SAM algorithm in MATLAB (MathWorks, Natick, MA), where reference spectra of two ROIs (plaque and either Tau or CAA) obtained from the same stack in ImageJ version 1.44e were imported from text files. In addition, an ROI corresponding to the background of the image was selected. The MATLAB script loaded the spectral stack, and for each pixel, it calculated the spectral angle (using SAM) between its spectral profile and the reference spectra (plaque, CAA or Tau, and background), thereby producing three SAM values. Of these values, the highest value was selected, which expressed the closest match to the respective reference spectrum. In essence, this procedure classified each pixel into one of the three categories. A new image was generated, by which each pixel is color coded according to the class it belongs to (green for plaque, red for Tau or CAA, and blue for background-like pixels). A threshold was set, so that only the highest-scoring pixels were displayed, and others were set to 0 (shown in black). This step is necessary because it eliminates pixels that score low compared with all three reference spectra, meaning that they were noisy or non-specific or the background had a peculiar spectral profile at that point. The threshold was experimentally determined and fixed at 0.95 (ie, extremely close to the maximum similarity of 1).

Results

hFTAA Passes the BBB and Stains Characteristic AD Lesions

Aged APP23 tg mice ($n = 5$), 20 to 22 months old, and symptomatic hemizygous or homozygous P301S Tau tg mice (hemizygous: $n = 3$, 14 to 15 months old; homozygous: $n = 6$, 6 months old) were i.v. injected with a single dose of 20 mg/kg hFTAA (Figure 1) and analyzed 24 hours later by assessing fluorescent emission on the respective brain sections. At this age, APP23 tg mice exhibited Aβ deposits in the brain parenchyma (Aβ plaques) and in the vasculature (CβAA),[22,28] whereas P301S Tau tg mice exhibited intracellular aggregates of hyperphosphorylated Tau.[23]

Histological analysis of hFTAA-injected APP23 mice revealed homogenous labeling of Aβ plaques and vascular CβAA throughout the brain. Depending on the age of the mice, Aβ plaques and CβAA of different severity grades were observed (Figure 2). In contrast, a cellular staining pattern of hFTAA was observed after peripheral hFTAA injection of hemizygous and homozygous P301S Tau tg mice. Although symptomatic homozygous P301S Tau tg mice depicted slightly more positive cells than

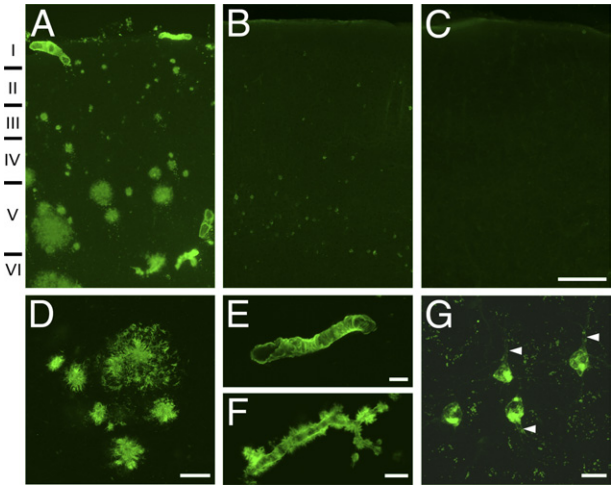

Figure 2. hFTAA passes the BBB and binds to amyloid lesions. At 24 hours after a single i.v. injection of hFTAA, characteristic amyloid lesions are labeled throughout the brain of transgenic mice. **A:** APP23 transgenic mice depict staining of Aβ plaques and CβAA. Imagery shows hFTAA staining in the cortex of a 21-month-old mouse. **B:** P301S Tau transgenic mice reveal staining of intracellular Tau aggregates. Cortical staining shows hFTAA-positive cells mainly in layers II and V. As one example, a 6-month-old homozygous mouse is shown. **C:** Wild-type animals depict no staining. **D–G:** High-magnification images of the different hFTAA-stained amyloid lesions. hFTAA staining of Aβ plaques (**D**), CβAA of different severity grades (**E** and **F**), and intracellular Tau aggregates (**G**). Protruding neurites are labeled (**arrowheads** in **G**). Small punctate staining in **G** reflects an unspecific autofluorescence signal of lipofuscin, a lipid degradation product frequently present in aged brain tissue. Images in **E–G** are maximum-intensity projections. Scale bars: 200 μm (**A–C**); 50 μm (**D** and **F**); 20 μm (**E** and **G**).

symptomatic hemizygous mice, no differences were present with respect to the staining pattern or the morphological characteristics of individual lesions. Positively stained cells were observed primarily in the brainstem and the amygdala, with additional staining in cortical neurons mostly in layers II and V (Figure 2). The cellular staining was mainly restricted to the soma and was absent in the nucleus. In some cases, protruding neurites were also stained (Figure 2G). Overall, the fluorescent staining distribution and morphological characteristics in APP23 and P301S Tau tg mice closely resembled the expected pathological characteristics previously described using immunohistological techniques in postmortem tissue.[22,23,28] Non-transgenic control mice depicted no staining after hFTAA injection (Figure 2).

To verify staining specificity at the cellular level, sections of hFTAA-injected APP23 and P301S Tau tg mice were postmortem labeled with antibodies directed against Aβ or hyperphosphorylated Tau (Figure 3). A close match of the two signals was observed. Visual inspection of Aβ labeling and the hFTAA signal revealed costaining of both Aβ plaques and CβAA ($n = 3$ APP23 tg mice, 21 to 22 months old). Regarding Tau lesions, the number of double-labeled cells in the neocortex ranged between 90% and 100% ($n = 4$ P301S Tau tg mice; hemizygous: $n = 1$, 14 months old; homozygous: $n = 3$, 6 months old; see *Materials and Methods* for technical details).

In additional experiments, sections of APP23 mice were postmortem labeled with either hFTAA or other well-known amyloid-specific dyes (Congo red, thioflavin S, or

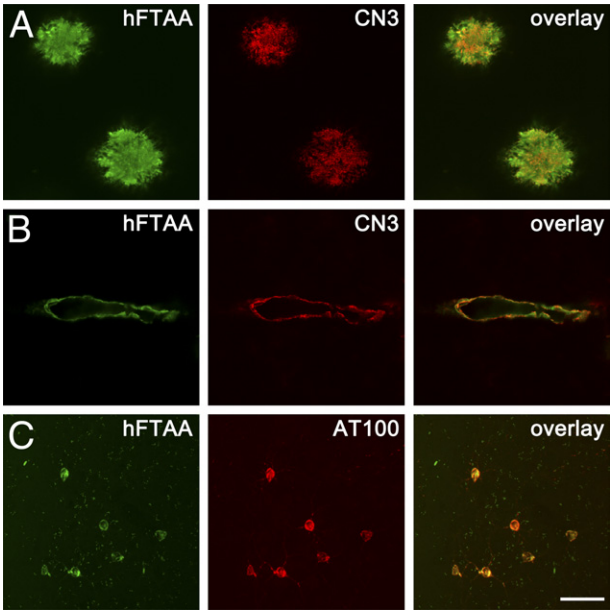

Figure 3. IHC costaining verifies hFTAA labeling of amyloid lesions. A close match of the hFTAA and IHC signal is observed for Aβ plaques (**A**) and CβAA (**B**), using the Aβ-specific antibody CN3. Imagery from an hFTAA-injected 21-month-old APP23 mouse. **C:** hFTAA staining shows a high portion of overlap with Tau-positive cells identified by an antibody directed against hyperphosphorylated Tau (AT100). Imagery from an hFTAA-injected 7-month-old homozygous P301S Tau tg mouse. Images are maximum-intensity projections. Scale bar = 50 μm (**A**–**C**).

methoxy-X04; Figure 4). Results revealed a similar staining pattern of Aβ plaques for hFTAA, methoxy-X04, and thioflavin S. While all these dyes stained the entire amyloid structure, Congo red only labeled the dense core of the Aβ deposits. hFTAA appeared to visualize the periphery of Aβ plaques particularly well, suggesting that it also stained diffuse amyloid.

Using Two-Photon Excitation hFTAA Spectrally Discriminates Amyloid Lesions

Spectral variations were analyzed in *ex vivo* brain sections of hFTAA-injected APP23 and P301S Tau tg mice using two-photon excitation at 780 nm (Figure 5; APP23 mice: n = 4, 20 to 21 months old; P301S Tau mice: hemizygous: n = 2, 15 months old; homozygous: n = 2, 6 months old). As no difference was observed between spectra from hemizygous and homozygous P301S Tau tg mice, the different genotypes were subsequently pooled. When hFTAA-labeled Tau aggregates were compared with hFTAA-labeled Aβ plaques, a distinct red shift of the hFTAA emission spectra was observed mainly within the right shoulder (up to 20 nm; Figure 5A). In addition, hFTAA-Tau spectra depicted a relative increase in the second peak at approximately 590 nm. Interindividual and intraindividual differences of hFTAA spectra acquired from the two pathological conditions are depicted in Figure 5B. Intraindividual differences of hFTAA bound to Aβ plaques (data from the four previously mentioned APP23 mice; 121 plaques in total) were minor and significantly less, compared with interindividual differences of spectra acquired from hFTAA bound to Tau aggregates (data from the four previously mentioned Tau mice; 163 Tau lesions in total). Care was taken to exclude hFTAA Tau spectra, which were contaminated by the presence of lipofuscin autofluorescence (see *Materials and Methods* for details). Thus, using two-photon excitation and systemic *in vivo* labeling, hFTAA spectrally discriminated the two hallmark lesions of AD, Aβ plaques and Tau aggregates.

Next, we assessed whether hFTAA had the potential to distinguish β-amyloid subtypes. Therefore, the spectra of hFTAA-bound Aβ plaques were compared with the spec-

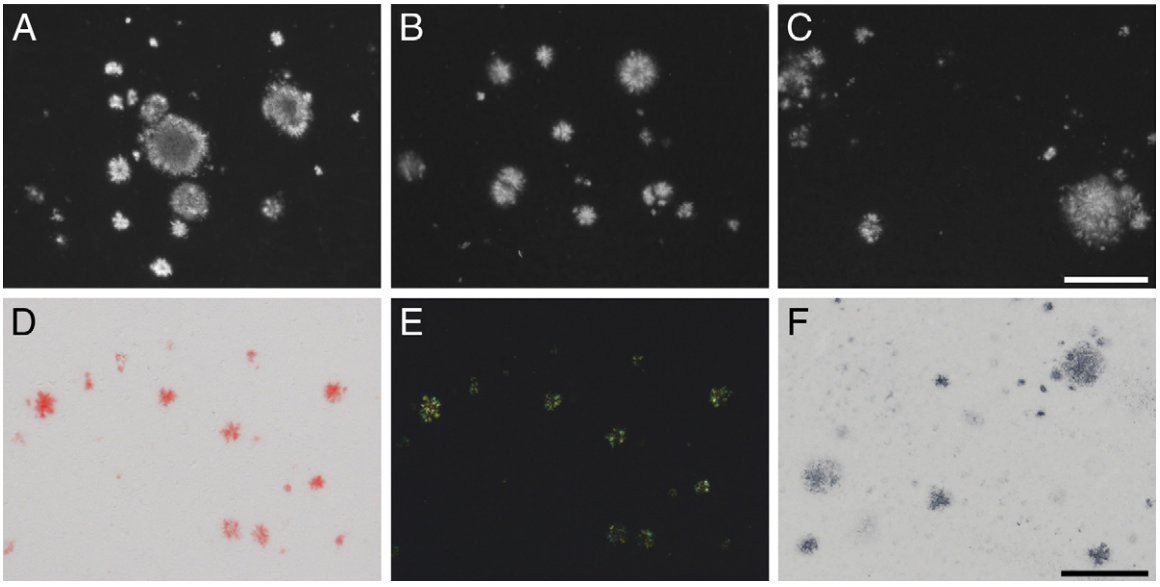

Figure 4. Comparison of hFTAA labeling with other amyloid-specific dyes and IHC staining of Aβ. Representative images of *ex vivo*–stained brain sections from an 18-month-old APP23 tg mouse. hFTAA (**A**), methoxy-X04 (**B**), and thioflavin S (**C**) depict labeling of Aβ plaques, including the plaque periphery, by which hFTAA stains the plaque periphery particularly well. In contrast, Congo red exclusively stains the compact plaque core [observed under transmitted (**D**) or polarized (**E**) light]. **F:** IHC staining with an Aβ-specific antibody (CN3) depicts labeling of the plaque core and periphery. Filters and imaging parameters were adjusted to ensure optimal display of stained structures regardless of differences in intensities. Scale bar = 200 μm.

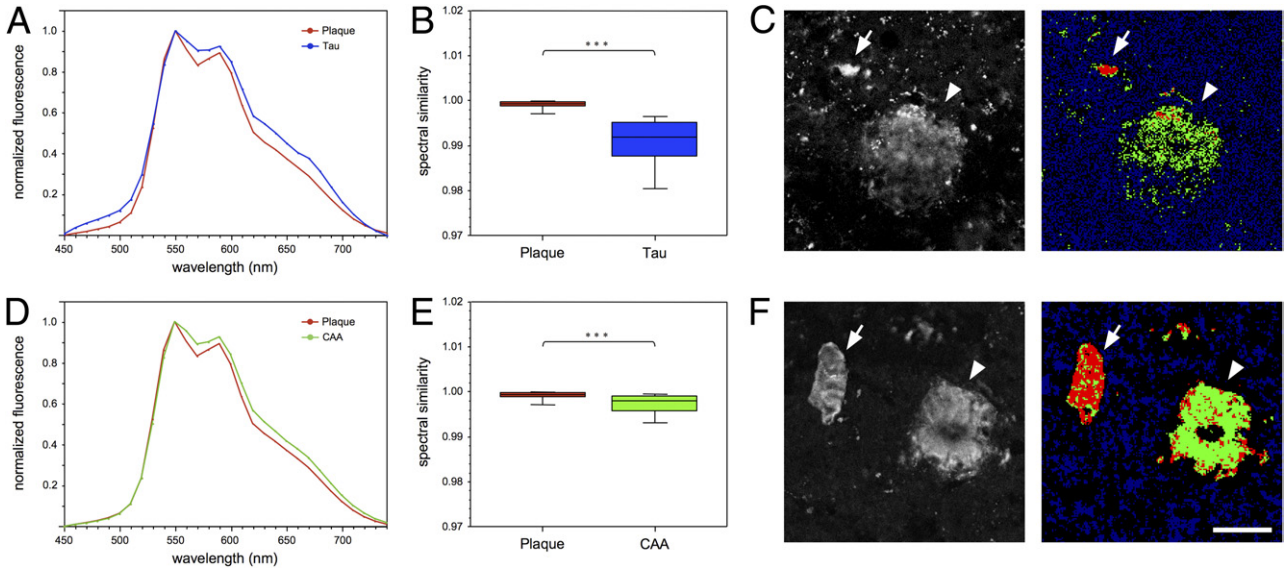

Figure 5. hFTAA spectrally discriminates different amyloid lesions. **A:** The mean normalized emission spectrum of hFTAA bound to Tau aggregates differs from the mean normalized hFTAA spectrum when bound to Aβ plaques. Analysis is performed on tissue of hFTAA-injected mice ($n = 4$ for both APP23 and P301S Tau mice; see *Results* for mice details) using two-photon excitation at 780 nm. **B:** Analysis of spectral similarity using the spectral angle mapper algorithm reveals that hFTAA Tau spectra are significantly different from hFTAA plaque spectra (previously mentioned mice; hFTAA spectra Tau: $n = 163$; hFTAA spectra plaque: $n = 121$; *U*-test; $P < 0.0001$). **C:** Two-photon image showing an example of neighboring hFTAA-stained Tau (**arrow**) and Aβ plaque (**arrowhead**) in a 17-month-old APP23 × P301S Tau double tg mouse. Spectral differences of the two lesions are displayed via automatic classification by the spectral angle mapper algorithm (pixels with the highest similarity to the plaque reference spectra are depicted in green; Tau, red; background-like pixels, blue; see *Materials and Methods* for details). **D:** Mean emission spectrum of hFTAA bound to CβAA differs from mean hFTAA spectrum bound to Aβ plaques. Analysis is performed on the tissue of hFTAA-injected APP23 mice ($n = 4$) using two-photon excitation at 780 nm. **E:** Analysis of spectral similarity using the spectral angle mapper algorithm shows that hFTAA CβAA spectra are significantly different from hFTAA plaque spectra (previously mentioned mice; hFTAA spectra CβAA: $n = 158$; hFTAA spectra plaque: $n = 121$; *U*-test, $P < 0.0001$). **F:** Two-photon image showing an example of neighboring hFTAA-stained CβAA (**arrow**) and Aβ plaque (**arrowhead**). Spectral differences of the two lesions are displayed via automatic categorization with the spectral angle mapper algorithm (pixels with highest similarity to the plaque reference spectra are depicted in green; CAA, red; background-like pixels, blue; see *Materials and Methods* for details). Scale bar = 50 μm (**C** and **F**). ***$P < 0.0001$ (**B** and **E**).

tra of hFTAA-bound CβAA in APP23 mice (data from four APP23 mice; 121 plaques and 158 CβAAs). Results revealed a red shift of the emission spectra for hFTAA when bound to CβAA compared with Aβ plaques, which was primarily evident in the right shoulder (up to 13 nm; Figure 5D). Overall, the observed spectral differences between CβAA and Aβ plaques were less pronounced than those observed between Aβ plaques and Tau lesions (Figure 5E). Nevertheless, these observations indicated that hFTAA could not only differentiate various amyloid types but also structural variances of the same protein.

The previously described results were collected from either APP23 or P301S Tau tg mice to ensure the purity of the collected spectra. To spectrally discriminate amyloid lesions within the same mouse, APP23 tg mice were crossed with P301S Tau tg mice to generate a model with mixed pathological characteristics. Again, hFTAA was injected i.v., and images containing Aβ and Tau lesions were captured from sections of the hFTAA-injected double tg mice (Figure 5, C and F; $n = 3$, 15 to 17 months old). Differences in the spectra of the distinct pathological conditions are displayed and color coded by a custom-made spectral classification algorithm (see *Materials and Methods* for details).

Discussion

Amyloid-specific ligands constitute an indispensable set of tools for the diagnosis, and the investigation of proteopathies, including AD. Since the initial description of the amyloid-binding dyes, Congo red and thioflavin T,[4,5] many amyloidotropic dyes have been developed with applications from basic science to clinical research. Despite the rapid progress in the field of *in vivo* amyloid imaging, limitations remain regarding specificity to individual amyloid types and conformational variants. In particular, cerebral proteopathies mostly consist of a mixture of various amyloids,[3] and dyes that can discriminate between such lesions and their conformational variants are of enormous diagnostic value and essential for studying disease pathomechanisms.

LCOs have unique optical properties, because they exhibit spectral changes when binding to distinct amyloid types.[18] The aim of the present study was to advance the use of LCOs to *in vivo* applications. The respective requirements were that the dye is able to do the following: i) pass the BBB, ii) bind amyloid lesions after peripheral application, and iii) exhibit lesion- and conformation-specific spectral shifts on two-photon excitation.

Herein, we have demonstrated that the heptameric LCO hFTAA fulfills all of these prerequisites when tested in mouse models of AD. After a single systemic injection, hFTAA crossed the BBB and specifically stained Aβ plaques, CβAA, and intracellular Tau lesions. Because the periphery of Aβ plaques was particularly well labeled with hFTAA, we expect that diffuse amyloid is also stained by hFTAA. This observation is consistent with a recent study[29] in which, and in contrast to thioflavin T, the

pentameric analogue of hFTAA (pFTAA[30]) stained diffuse amyloid deposits in the striatum of bitransgenic ArcSwe × tg-Swe mice. Notably, several LCOs, including hFTAA, also detected non-thioflavinophilic prefibrillar amyloid species *in vitro*,[20] demonstrating that LCOs have the potential to visualize protein aggregates that are not detected by classic amyloid-specific dyes, such as thioflavin T.

In addition to the *in vivo* labeling of all major AD pathological characteristics, hFTAA allowed the spectral discrimination of the amyloid lesions on two-photon excitation, albeit demonstrated in *ex vivo* tissue. *In vivo* two-photon spectral imaging is limited by the lack of commercially available spectral detectors that are optimized for *in vivo* applications (ie, the current detectors lack the required sensitivity). However, new customized spectral detectors are developed, which will offer improved sensitivity and allow spectral analysis of different amyloid lesions *in vivo*.

The spectral shift of hFTAA bound to Tau versus Aβ plaques observed in the present article is similar to the spectral shift using single-photon excitation previously reported by Klingstedt et al.[20] In the latter study, pFTAA depicted an even bigger spectral shift between the two pathological features, but only when combining emission spectra acquired with two different excitation wavelengths. Because we focused on the usability for *in vivo* application, sequential excitation with different wavelengths was not deemed practical (eg, because of enhanced phototoxicity).

Amyloidotrophic dyes potentially interfere with amyloid growth. In PS1/APP tg mice, methoxy-X04 has interfered with Aβ plaque formation, albeit in higher doses, as normally used for imaging (20 mg/kg, treatment from the age of 9 weeks, three times a week, nine treatments in total).[31] Therefore, it is of specific interest that the persistent treatment with the pentameric oligothiophene pFTAA revealed no effect on Aβ load in APPPS1 tg mice (10 mg/kg, four initial daily injections, followed by weekly injections from the age of 42 to 120 days)[32] and in APP23 tg mice (10 mg/kg, two initial daily injections, followed by biweekly injections from the age of 6 to 13 months; own unpublished data). Furthermore, no signs of toxicity were observed with respect to body weight, differential blood cell counts, and histological analyses of peripheral organs.[32] Assuming analogy with its heptameric form, these results emphasize the suitability of hFTAA as a long-term *in vivo* imaging probe. This observation also suggests that pFTAA (and presumably hFTAA) binds to the amyloid backbone and does not interfere with the growth of the steric zipper.[3]

There are multiple lines of evidence that amyloid lesions in the brain are structurally diverse, ranging from different Aβ plaque morphotypes and Tau inclusion bodies to various soluble structurally distinct oligomeric species with presumably different biological activities.[3,33] Thus, by introducing different mouse models and age groups, future studies will assess whether hFTAA is also effective in distinguishing these conformational variants and whether changes in amyloid composition/structure can be visualized with disease progression in the living organism.

The present study establishes the baseline for such future intravital applications. Herein, we describe, for the first time to our knowledge, a conformation-sensitive dye, which, on peripheral application, labels extracellular plaques, CβAA, and intracellular Tau lesions. Furthermore, we demonstrated that these different amyloid lesions can be spectrally discriminated using two-photon excitation, thus paving the way for *in vivo* spectral imaging and differentiation of amyloid lesions over time. The effective separation of amyloid (sub) types may allow for the linkage of distinct conformational amyloid structures to *in vivo* malfunctions.

Acknowledgments

We thank Andrea Bosch, Ulrike Obermüller, Christian Krüger, Carina Leibssle, Michael Hruscha, and Jörg Odenthal for technical support, Mikael Lindgren and Nina Reitan (Trondheim, Norway) for helpful discussions on 2P fluorescence parameters, Matthias Staufenbiel (Basel, Switzerland) for providing the APP23 transgenic line, and Michel Goedert (Cambridge, UK) for providing the P301S Tau transgenic line.

References

1. Chiti F, Dobson CM: Protein misfolding, functional amyloid, and human disease. Annu Rev Biochem 2006, 75:333–366
2. Selkoe DJ: Folding proteins in fatal ways. Nature 2003, 426:900–904
3. Eisenberg D, Jucker M: The amyloid state of proteins in human diseases. Cell 2012, 148:1188–1203
4. Bennhold H: Eine spezifische Amyloidfärbung mit Kongorot. Münch Med Wochenschr 1922, 69:1537–1538
5. Vassar PS, Culling CF: Fluorescent stains, with special reference to amyloid and connective tissues. Arch Pathol 1959, 68:487–498
6. Reinke AA, Gestwicki JE: Insight into amyloid structure using chemical probes. Chem Biol Drug Des 2011, 77:399–411
7. Klunk WE, Engler H, Nordberg A, Wang Y, Blomqvist G, Holt DP, Bergstrom M, Savitcheva I, Huang GF, Estrada S, Ausen B, Debnath ML, Barletta J, Price JC, Sandell J, Lopresti BJ, Wall A, Koivisto P, Antoni G, Mathis CA, Langstrom B: Imaging brain amyloid in Alzheimer's disease with Pittsburgh Compound-B. Ann Neurol 2004, 55:306–319
8. Weiner MW, Aisen PS, Jack CR Jr, Jagust WJ, Trojanowski JQ, Shaw L, Saykin AJ, Morris JC, Cairns N, Beckett LA, Toga A, Green R, Walter S, Soares H, Snyder P, Siemers E, Potter W, Cole PE, Schmidt M; Alzheimer'S Disease Neuroimaging Initiative: The Alzheimer's disease neuroimaging initiative: progress report and future plans. Alzheimers Dement 2010, 6:202–211.e7
9. Morris JC, Roe CM, Grant EA, Head D, Storandt M, Goate AM, Fagan AM, Holtzman DM, Mintun MA: Pittsburgh compound B imaging and prediction of progression from cognitive normality to symptomatic Alzheimer disease. Arch Neurol 2009, 66:1469–1475
10. Klunk WE, Bacskai BJ, Mathis CA, Kajdasz ST, McLellan ME, Frosch MP, Debnath ML, Holt DP, Wang Y, Hyman BT: Imaging Abeta plaques in living transgenic mice with multiphoton microscopy and methoxy-X04, a systemically administered Congo red derivative. J Neuropathol Exp Neurol 2002, 61:797–805
11. Dong J, Revilla-Sanchez R, Moss S, Haydon PG: Multiphoton in vivo imaging of amyloid in animal models of Alzheimer's disease. Neuropharmacology 2010, 59:268–275
12. Hefendehl JK, Wegenast-Braun BM, Liebig C, Eicke D, Milford D, Calhoun ME, Kohsaka S, Eichner M, Jucker M: Long-term in vivo imaging of beta-amyloid plaque appearance and growth in a mouse model of cerebral beta-amyloidosis. J Neurosci 2011, 31:624–629
13. Toyama BH, Weissman JS: Amyloid structure: conformational diversity and consequences. Annu Rev Biochem 2011, 80:557–585

14. Jucker M, Walker LC: Pathogenic protein seeding in Alzheimer disease and other neurodegenerative disorders. Ann Neurol 2011, 70: 532–540
15. Levine H 3rd, Walker LC: Molecular polymorphism of Abeta in Alzheimer's disease. Neurobiol Aging 2010, 31:542–548
16. Duyckaerts C, Delatour B, Potier MC: Classification and basic pathology of Alzheimer disease. Acta Neuropathol 2009, 118:5–36
17. Viswanathan A, Greenberg SM: Cerebral amyloid angiopathy in the elderly. Ann Neurol 2011, 70:871–880
18. Klingstedt T, Nilsson KP: Conjugated polymers for enhanced bioimaging. Biochim Biophys Acta 2011, 1810:286–296
19. Nilsson KP, Aslund A, Berg I, Nystrom S, Konradsson P, Herland A, Inganas O, Stabo-Eeg F, Lindgren M, Westermark GT, Lannfelt L, Nilsson LN, Hammarstrom P: Imaging distinct conformational states of amyloid-beta fibrils in Alzheimer's disease using novel luminescent probes. ACS Chem Biol 2007, 2:553–560
20. Klingstedt T, Aslund A, Simon RA, Johansson LB, Mason JJ, Nystrom S, Hammarstrom P, Nilsson KP: Synthesis of a library of oligothiophenes and their utilization as fluorescent ligands for spectral assignment of protein aggregates. Org Biomol Chem 2011, 9:8356–8370
21. Sigurdson CJ, Nilsson KP, Hornemann S, Manco G, Polymenidou M, Schwarz P, Leclerc M, Hammarstrom P, Wuthrich K, Aguzzi A: Prion strain discrimination using luminescent conjugated polymers. Nat Methods 2007, 4:1023–1030
22. Sturchler-Pierrat C, Abramowski D, Duke M, Wiederhold KH, Mistl C, Rothacher S, Ledermann B, Burki K, Frey P, Paganetti PA, Waridel C, Calhoun ME, Jucker M, Probst A, STaufenbiel M, Sommer B: Two amyloid precursor protein transgenic mouse models with Alzheimer disease-like pathology. Proc Natl Acad Sci U S A 1997, 94:13287–13292
23. Allen B, Ingram E, Takao M, Smith MJ, Jakes R, Virdee K, Yoshida H, Holzer M, Craxton M, Emson PC, Atzori C, Migheli A, Crowther RA, Ghetti B, Spillantini MG, Goedert M: Abundant Tau filaments and nonapoptotic neurodegeneration in transgenic mice expressing human P301S Tau protein. J Neurosci 2002, 22:9340–9351
24. Eisele YS, Obermuller U, Heilbronner G, Baumann F, Kaeser SA, Wolburg H, Walker LC, STaufenbiel M, Heikenwalder M, Jucker M: Peripherally applied Abeta-containing inoculates induce cerebral beta-amyloidosis. Science 2010, 330:980–982
25. de Carvalho OA Jr, Meneses PR: Spectral correlation mapper (SCM): an improvement on the spectral angle mapper (SAM). Summaries of the 9th airborne earth science workshop. Pasadena, CA: JPL Publication 00–18 (2000).
26. Dennison PE, Halligan KQ, Roberts DA: A comparison of error metrics and constraints for multiple endmember spectral mixture analysis and spectral angle mapper. Remote Sens Environ 2004, 93:359–367
27. Shafri HZM, Suhaili A, Mansor S: The performance of maximum likelihood: spectral angle mapper, neural network and decision tree classifiers in hyperspectral image analysis. J Comput Sci 2007, 3:419–423
28. Calhoun ME, Burgermeister P, Phinney AL, Stalder M, Tolnay M, Wiederhold KH, Abramowski D, Sturchler-Pierrat C, Sommer B, STaufenbiel M, Jucker M: Neuronal overexpression of mutant amyloid precursor protein results in prominent deposition of cerebrovascular amyloid. Proc Natl Acad Sci U S A 1999, 96:14088–14093
29. Lord A, Philipson O, Klingstedt T, Westermark G, Hammarstrom P, Nilsson KP, Nilsson LN: Observations in APP bitransgenic mice suggest that diffuse and compact plaques form via independent processes in Alzheimer's disease. Am J Pathol 2011, 178:2286–2298
30. Aslund A, Sigurdson CJ, Klingstedt T, Grathwohl S, Bolmont T, Dickstein DL, Glimsdal E, Prokop S, Lindgren M, Konradsson P, Holtzman DM, Hof PR, Heppner FL, Gandy S, Jucker M, Aguzzi A, Hammarstrom P, Nilsson KP: Novel pentameric thiophene derivatives for in vitro and in vivo optical imaging of a plethora of protein aggregates in cerebral amyloidoses. ACS Chem Biol 2009, 4:673–684
31. Cohen AD, Ikonomovic MD, Abrahamson EE, Paljug WR, Dekosky ST, Lefterov IM, Koldamova RP, Shao L, Debnath ML, Mason NS, Mathis CA, Klunk WE: Anti-amyloid effects of small molecule Abeta-binding agents in PS1/APP mice. Lett Drug Des Discov 2009, 6:437
32. Handrick S, Prokop S, Nystrom S, Mason JJ, Reitan NR, Wegenast-Braun BM, Lindgren M, Jucker M, Nilsson KP, Hammarstrom P, Heppner FL: Luminescent Conjugated Oligothiophenes (LCOs) as Pharmacophores in Alzheimer's Disease. Paris, Fondation Ipsen, 2012
33. Larson ME, Lesne SE: Soluble Abeta oligomer production and toxicity. J Neurochem 2012, 120(Suppl 1):125–139